Transfer Nuclear Overhauser Effect Study of the Conformation of Oxytocin Bound to Bovine Neurophysin I†

G. Lippens,*,‡,§ K. Hallenga,*,‖ D. Van Belle,‡ S. J. Wodak,‡ N. R. Nirmala,⊥ P. Hill,● K. C. Russell,● D. D. Smith,● and V. J. Hruby●

UCMB and Corvas at UCMB, Free University of Brussels, Av. P. Hêger CP160/16, 1050 Brussels, Belgium, Laboratorium voor Genetika, Universiteit Gent, Ledeganckstraat 35, 9000 Ghent, Belgium, Department of Biological Chemistry and Molecular Pharmacology, Harvard Medical School, 240 Longwood Avenue, Boston, Massachusetts 02115, and Department of Chemistry, University of Arizona, Tucson, Arizona 85721

Received February 24, 1993; Revised Manuscript Received June 7, 1993

ABSTRACT: This study reports the structure of the peptide hormone oxytocin bound to its carrier protein, neurophysin I, obtained by nuclear magnetic resonance techniques. At the pH value of 2.1 in our experiments, the ligand is in fast exchange with its carrier protein, allowing the use of transfer-NOE methods. The number of distance constraints for the peptide being limited, considerable attention has been paid to an accurate distance determination. The resulting accurate distance limits were used as input for a distance geometry calculation followed by a restrained molecular dynamics run. Convergence to a well-defined family of structures for oxytocin in its bound state was reached. Both the backbone and the side-chain conformations differ between the bound form and the crystal structure of free oxytocin [Wood, S. P., *et al.* (1986) *Science 232*, 633]. These differences, as well as other structural features of the bound form, are discussed in terms of interactions made with the carrier protein. Transfer-NOE experiments at low peptide protein ratios provide direct experimental evidence for contacts between the oxytocin Tyr^2 residue and an aromatic residue of neurophysin. The resonance assignments of the aromatic groups [Whittaker, B. A., *et al.* (1985) *Biochemistry 24*, 2782] together with the recently published X-ray structure of the neurophysin II protein complexed with a dipeptide [Chen et al. (1991) *Proc. Natl. Acad. Sci. U.S.A. 88*, 4240] allow us to assign the aromatic signal on the protein to the neurophysin Phe^{22} residue.

Detailed knowledge of the three-dimensional structure of a protein–ligand complex, be it that of an enzyme with its substrate or of a hormone with its receptor, is a prerequisite for understanding the biological function mediated by the association. Earlier studies, mostly of complexes between proteolytic enzymes and proteinase inhibitors (Blow, 1976; Huber & Bode, 1978; Hubbard *et al.*, 1991) and of an antibody–protein complex (Amit *et al.*, 1986) supported the view of a rigid lock-and-key complementarity. This view, however, has been increasingly challenged by subsequent studies which showed that proteins can change their conformations substantially upon ligand binding (Bennett & Huber, 1984; Weber P. C., *et al.*, 1991). Moreover, recent studies have demonstrated that the ligands can also undergo profound conformational changes upon binding to their receptor proteins (Weber C., *et al.*, 1991; Fesik *et al.*, 1991; Rini *et al.*, 1992). Such changes are most likely to occur in ligands such as short peptides that tend to display considerable conformational flexibility when free in aqueous or organic solutions (Hruby, 1974; Knappenberg *et al.*, 1982). Trying to derive knowledge on the structure of the complex from structural data on the free protein and ligand components is therefore not always meaningful, as there is no way to tell from such data which of the observed conformations of the free peptide is biologically relevant or what conformational transition will occur in the protein upon binding. To obtain this valuable information requires direct analysis of the 3D structure and interactions of the bound species.

X-ray crystallography of the molecular complex has been the method of choice for performing such analyses [Knighton *et al.*, 1991; Fremont *et al.*, 1992; an overview of all recent structures of complexes determined by X-ray crystallography is given by Hendrickson and Wüthrich (1992)]. High-resolution nuclear magnetic resonance (NMR) spectroscopy, performed with ^{13}C-, ^{15}N-, or ^{19}F-enriched ligands also has provided valuable information on the interactions made by the bound species, and recently, new multidimensional NMR techniques combining the use of isotopically enriched molecules with isotope editing schemes have allowed the determination of the structures of bound ligand molecules (Weber, C., *et al.*, 1991; Fesik *et al.*, 1991) and of whole complexes (Puglisi *et al.*, 1992; Ikura *et al.*, 1992). However, the bulk of the performed studies concern complexes with high association constants, the reason being that the crystallization of complexes with low association constants is often a problem, and NMR methods require that the complex be the major molecular species over the time scale of the experiment.

An alternative NMR method applicable to relatively weak complexes was initially suggested by Balaram, Bothner-By, and Dadok (Balaram *et al.*, 1972a,b) and subsequently developed theoretically by Clore and Gronenborn (Clore & Gronenborn, 1982, 1983). This method is based on the chemical exchange mediated transfer of the NOE cross peak magnetization from the bound to the free ligand molecule, where it can be readily observed. Numerous studies have used this technique to gather information about the bound form of the ligand (Hallenga *et al.*, 1988; Ni *et al.*, 1989,

† G.L. was supported by a fellowship of the Belgian National Science Foundation [National Fonds voor Wetenschappelijk Onderzoek (NFWO)]. This research was supported by a grant from the U.S. Public Health Service, D/C 17420.

* Authors to whom correspondence should be addressed.
‡ UCMB, Free University of Brussels.
§ Universiteit Gent.
‖ Corvas at UCMB, Free University of Brussels.
⊥ Harvard Medical School.
● University of Arizona.

0006-2960/93/0432-9423$04.00/0

1990; Anglister & Zilber, 1990; Bevilacqua *et al.*, 1990; Campbell & Sykes, 1991). Obtaining an accurate structural model, however, remains difficult owing mainly to the limited number of experimental constraints that can be deduced from transfer-NOE studies. This situation is very different from that in studies of globular proteins, where the compact molecular core provides numerous NOE constraints per residue. A bound ligand shows a closer analogy to residues at the protein surface for which available techniques such as distance geometry (Crippen & Havel, 1988) and/or restrained molecular dynamics (Kaptein *et al.*, 1985) often fail to yield a satisfying solution because the problem is underdetermined.

In this study, we apply the transfer-NOE technique to the oxytocin–neurophysin system. The peptide hormones oxytocin (H-Cys-Tyr-Ile-Gln-Asn-Cys-Pro-Leu-Gly-NH2) and arginine vasopressin (H-Cys-Tyr-Phe-Gln-Asn-Cys-Pro-Arg-Gly-NH2) are synthesized principally within the hypothalamus of the posterior pituitary axis, each as part of a common precursor with their associated carrier protein neurophysin. The major processing of the precursor molecules into hormone and neurophysin occurs subsequent to their packaging into neurosecretory granules (Gainer *et al.*, 1985). The interactions between the hormone and neurophysin segments in the precursor are similar to the ones in the processed hormone–neurophysin complexes. The oxytocin-specific neurophysin I (NP I) and the vasopressin-specific neurophysin II (NP II) show a very high degree of sequence homology (Capra et al., 1972). This homology is accompanied by almost identical hormone-binding and self-association properties *in vitro* (Breslow & Walter, 1972; Breslow, 1979). Though neurophysin is not the actual receptor for the hormones but rather serves as a carrier of the hormones in the neurosecretory granules, the complex with the hormone provides a unique system for investigating the general properties of peptide hormone–macromolecule interactions. Because the protein can be isolated in pure form in gram quantities and very high purity hormones are available by direct synthesis, allowing for the insertion of isotope-labeled residues, several nuclear magnetic resonance studies [e.g., Blumenstein *et al.* (1979, 1984), Hallenga *et al.* (1988), and Live *et al.* (1987)] as well as studies involving the binding of hormone analogues to neurophysins [for a review, see Breslow and Burman (1990)] have been carried out on this system. The main conclusion is that the peptide residues 1 and 2, and to a lesser extent residue 3, are essential for the hormone–NP interaction. Recently, the structure of a complex of neurophysin II and a dipeptide has been determined by X-ray crystallography (Chen *et al.*, 1991), providing information on the location and conformation of the binding site on the neurophysin.

Here we complement the above information with a report on gathering accurate distance constraints for the bound ligand. Because at low pH the oxytocin–neurophysin exchange rate becomes fast, these distances could be obtained by transfer-NOE techniques. We construct a model for the oxytocin molecule bound to neurophysin. The resulting structure differs from the crystal structure of the free oxytocin molecule, both in the conformation of the backbone (ϕ,ψ) angles and of the side-chain χ angles. Moreover, our analysis provides information on specific proton–proton contacts between the oxytocin and NP I molecule, which together with the detailed description of the structure of the bound hormone should be helpful in deriving a detailed atomic description of the complex using molecular modeling techniques.

MATERIALS AND METHODS

Sample Preparation. Highly purified oxytocin (>99%) was prepared by direct chemical synthesis as previously reported (Upson & Hruby, 1976). The neurophysin I (NP I) proteins were isolated from freeze-dried bovine pituitaries and purified as previously described (Blumenstein & Hruby, 1976).

NMR Experiments. The spectral assignments of the oxytocin proton resonances in aqueous solution were determined previously (Brewster & Hruby, 1973) and were verified in the presence of neurophysin by Nirmala (Nirmala, 1987). NOESY spectra of the free peptide in solution gave no cross peaks due to the correlation time effect, and dipolar correlated spectra in the rotating frame (ROESY) (Bothner-By *et al.*, 1984) only gave intraresidue cross peaks, indicating that the peptide is flexible in solution, as was previously emphased (Brewster & Hruby, 1973). NOESY spectra of oxytocin in the presence of neurophysin I were recorded with six different mixing times ranging from 40 to 240 ms on a Varian Unity 600-MHz spectrometer, using detection with spin echo to improve the baseline properties (Lippens & Hallenga, 1990). The transfer-ROESY experiments were performed with a spin-lock field of γB_1 = 6.19 kHz. Concentrations used were 0.8 mM neurophysin and 8 mM oxytocin, in a mixture of 90% H_2O–10% D_2O. Data sets of 512 by 2048 points were acquired with a sweep width of 7200 Hz. One level of zero-filling and multiplication with a shifted Gaussian filter were applied in both dimensions prior to Fourier transformation. Parameters were 53 ms for the width at half-height and 5 ms for the origin shift in the ω_2 direction and 15 ms and 3 ms in the ω_1 direction. The temperature was 22 °C, and the pH was brought to 2.1 to prevent precipitation. A value of 60 s^{-1} for the exchange rate was estimated from the exchange-mediated line broadening of the Tyr^2 ϵ and the Asn^5 NH resonances (Pople *et al.*, 1959).

Measurements of coupling constants at different peptide–protein concentrations and a subsequent extrapolation to a 1:1 concentration have also been used to get information about dihedral angles in the bound conformation (Campbell & Sykes, 1991). We measured the splittings of the amide protons for different peptide concentrations (keeping the protein concentration constant) up to a 4:1 sample but found no substantive differences in the coupling constants. Therefore, these data were not used in the subsequent structure determination.

Structure Determination. (*a*) *Derivation of Distance Constraints.* For studies of globular proteins, one usually divides the distances into rather coarse groups according to strong, medium, or weak intensities of the cross peaks. This limited accuracy of the distance classification does not prevent convergence of algorithms to well-defined structures, as long as the number of constraints is sufficiently large (Wagner *et al.*, 1987). The number of (transfer) NOEs in our case of a small molecule being more limited, we directed our efforts to a more accurate distance determination. Buildup curves of the transferred magnetization were constructed from six NOE experiments with mixing times ranging from 40 to 240 ms. In each of the 2D NOE and ROE experiments the evaluation of the cross-peak volumes was carried out by defining a rectangle around each peak and using the volume integration routines provided by Varian. To improve the linearity of the buildup curves, we normalized the intensity of the cross peaks with respect to the volumes of the corresponding diagonal peaks (Macura *et al.*, 1986). Because of overlap problems on the diagonal, we calculated the volume of a diagonal peak from its height and the width measured on two or more cross peaks (Fejzo *et al.*, 1990). This method reduces the problem

Table I: Chemical Shift Values (ppm) of All Proton Resonances of the Bound Oxytocin Molecule, as Well as Upper and Lower Limits for the Distance Restraints Used as Input for the Distance Geometry Algorithm To Get a Structure Model[a]

diagonal peak assignments			corresponding cross peaks			distance between protons, upper and lower limits (Å)
residue	proton	freq diagonal peak (ppm)	freq cross peak (ppm)	residue	proton	
Cys[1]	α	4.26	3.44	Cys[1]	β1	3.0–2.0
			3.28	Cys[1]	β2	3.0–2.0
			8.99	Tyr[2]	NH	2.5–2.1
	β1	3.45	3.26	Cys[1]	β2	1.8–1.8
			8.99	Tyr[2]	NH	3.3–2.6
	β2	3.28	8.99	Tyr[2]	NH	3.0–2.2
Tyr[2]	α	4.78*	3.14	Tyr[2]	β1	3.5–2.0
			7.20	Tyr[2]	δ	4.0–2.0
			7.96	Ile[3]	NH	3.5–2.0
	β1	3.14	2.97	Tyr[2]	β2	1.8–1.8
			7.20	Tyr[2]	δ	4.0–2.0
			8.99	Tyr[2]	NH	3.2–2.4
			7.96	Ile[3]	NH	3.1–2.2
	β2	2.97	7.20	Tyr[2]	δ	4.0–2.0
			8.99	Tyr[2]	NH	2.7–2.0
			7.96	Ile[3]	NH	3.8–2.8
	δ	7.20	6.86	Tyr[2]	ε	2.5–2.5
			8.99	Tyr[2]	NH	3.0–2.3
			0.87	Ile[3]	γ2 (CH3)	5.0–2.0
			1.19	Ile[3]	γ11 (CH2)	5.0–2.0
			2.84	Asn[5]	β1,β2	4.0–2.5
	ε	6.86	0.87	Ile[3]	γ2 (CH3)	5.0–2.0
	NH	8.99	7.96	Ile[3]	NH	3.3–2.8
			2.84	Asn[5]	β1,β2	4.1–3.1
Ile[3]	α	4.02	1.88	Ile[3]	β	2.7–2.1
			0.87	Ile[3]	γ2 (CH3)	5.0–2.0
			1.19	Ile[3]	γ1 (CH2)	3.5–2.0
			1.00	Ile[3]	γ2 (CH2)	4.0–2.0
			7.96	Ile[3]	NH	2.7–2.1
			8.20	Gln[4]	NH	2.7–2.1
	β	1.88	0.87	Ile[3]	γ2 (CH3)	
			1.19	Ile[3]	γ11 (CH2)	3.0–2.0
			1.00	Ile[3]	γ12 (CH2)	4.0–2.0
			7.96	Ile[3]	NH	2.6–2.0
			8.19	Gln[4]	NH	3.0–2.3
	γ11 (CH2)	1.19	0.87	Ile[3]	γ2 (CH3)	
			0.83	Ile[3]	δ (CH3)	
			7.96	Ile[3]	NH	4.5–2.0
			8.19	Gln[4]	NH	
	γ2 (CH3)	0.95	1.89	Ile[3]	β	5.0–2.0
			1.18	Ile[3]	γ1	5.0–2.0
			8.19	Gln[4]	NH	4.0–2.0
			0.83	Ile[3]	δ (CH3)	
	δ (CH3)	0.83				
	NH	7.94	8.19	Gln[4]	NH	4.0–2.0
Gln[4]	α	4.10	2.04	Gln[4]	β1,β2	3.5–2.0
			2.38	Gln[4]	γ1,γ2	5.0–2.0
			8.19	Gln[4]	NH	2.6–2.1
			8.32	Asn[5]	NH	2.9–2.3
	β1,β2	2.04	2.38	Gln[4]	γ1,γ2	5.0–2.0
			8.19	Gln[4]	NH	2.8–2.0
			8.32	Asn[5]	NH	3.4–2.4
	γ1,γ2	2.38	8.19	Gln[4]	NH	5.0–2.0
			6.88	Gln[4]	NH2	5.0–2.0
			7.60	Asn[5]	NH2	5.0–2.0
	NH	8.19	8.32	Asn[5]	NH	5.0–3.0
Asn[5]	α	4.72*	2.82	Asn[5]	β1,β2	5.0–2.0
	β1,β2	2.82	8.32	Asn[5]	NH	3.1–2.1
			7.60	Asn[5]	NH2	4.0–2.5
			8.19	Cys[6]	NH	3.3–2.5
	NH	8.32	2.94	Cys[6]	β2	5.0–2.0
			8.19	Cys[6]	NH	2.4–2.0
Cys[6]	α	4.85*	3.44	Cys[1]	β1	4.5–2.5
			3.28	Cys[1]	β2	3.0–2.0
			3.21	Cys[6]	β1	4.0–2.0
			2.94	Cys[6]	β2	4.0–2.0
			3.74	Pro[7]	δ1	3.0–2.0
			3.68	Pro[7]	δ2	3.0–2.0
	β1	3.21	2.94	Cys[6]	β2	1.8–1.8
			8.19	Cys[6]	NH	3.2–2.3
			3.74	Pro[7]	δ1	5.0–2.5
			3.68	Pro[7]	δ2	5.0–2.5
	β2	2.93	8.19	Cys[6]	NH	2.7–2.0
	NH	8.19	3.74	Pro[7]	δ1	5.0–2.0

Table I: (Continued)

diagonal peak assignments			corresponding cross peaks			distance between protons, upper and lower limits (Å)
residue	proton	freq diagonal peak (ppm)	freq cross peak (ppm)	residue	proton	
			3.68	Pro^7	δ2	5.0–2.0
Pro^7	α	4.41	2.28	Pro^7	β1	4.0–2.0
			1.90	Pro^7	β2	4.0–2.0
			2.02	Pro^7	γ1,γ2	5.0–2.0
			8.48	Leu^8	NH	2.6–2.0
			8.37	Gly^9	NH	5.0–2.0
	β1	2.28	1.90	Pro^7	β2	1.8–1.8
			2.02	Pro^7	γ1,γ2	3.0–2.0
			3.75	Pro^7	δ1	4.0–2.0
			3.69	Pro^7	δ2	4.0–2.0
			8.48	Leu^8	NH	5.0–2.5
	β2	1.90	2.02	Pro^7	γ1,γ2	3.0–2.0
			3.75	Pro^7	δ1	4.0–2.0
			3.69	Pro^7	δ2	4.0–2.0
			8.48	Leu^8	NH	5.0–2.5
	γ1,γ2	2.02	3.75	Pro^7	δ1	3.0–2.0
			3.69	Pro^7	δ2	3.0–2.0
			8.48	Leu^8	NH	5.0–2.0
	δ1	3.75	3.69	Pro^7	δ2	1.8–1.8
	δ2	3.69				
Leu^8	α	4.29	1.65	Leu^8	β1	4.0–2.0
			1.60	Leu^8	β2	4.0–2.0
			0.91	Leu^8	γ	5.0–2.0
			0.86	Leu^8	δ (CH3)	4.5–2.0
	β1	1.65	1.60	Leu^8	β2	1.8–1.8
			0.91	Leu^8	γ	4.0–2.0
			0.86	Leu^8	δ (CH3)	4.5–2.0
	β2	1.60	0.91	Leu^8	γ	4.0–2.0
			0.86	Leu^8	δ (CH3)	4.5–2.0
	γ	0.91	0.86	Leu^8	δ (CH3)	4.0–2.0
	NH	8.48	8.37	Gly^9	NH	4.0–2.0
Gly^9	α1	3.93	8.37	Gly^9	NH	3.5–2.0
	α2	3.86	8.37	Gly^9	NH	3.5–2.0
	NH	8.37				

[a] All data come from a series of NOESY spectra at 22 °C (with six different mixing times between 40 and 240 ms, except for the α protons that fall under the water line at this temperature. For protons marked with an asterisk (*), resonance frequencies were determined at 50 °C.

of overlap on the diagonal, as the height of a peak is less sensitive to an offset than its volume integral. For the isolated Tyr^2 δ proton resonance, we compared calculated volumes to the values obtained by direct volume integration. The ratio of both integral values stayed constant to within 10% over the whole range of mixing times. Using the values of the volume integrals obtained by direct integration, we measured a buildup rate of 0.14 s^{-1} for the cross peak between the δ and ε protons of the Tyr^2 residue. This value must be corrected by the factor $f/(1+f)$ to find the real cross relaxation rate, where f is the ratio of the concentration of bound hormone to the concentration of free hormone at chemical equilibrium (Landy & Rao, 1991; Lippens *et al.*, 1992). With a value of 0.11 for f (initial 10:1 ratio of hormone to protein), we find a value of 1.4 s^{-1} for R_{IS}, which, together with a distance of 2.47 Å between the protons, leads to a correlation time, τ_c, of 5.7 ns, whereas a value of 10 ns would be expected on the basis of the molecular weight of the complex (Hallenga & Koenig, 1976). In a similar way, we measured the cross-relaxation rate for three other pairs of geminal protons (all side chains of residues in the ring part of oxytocin) and found correlation times ranging from 5.3 to 6.2 ns. An alternative calculation of the correlation times based on a comparison of NOE and ROE buildup rates confirmed these values (Lippens *et al.*, 1992). Large variations in correlation times that might lead to erroneous results in an accurate determination of distances can thus be excluded, at least for the backbone of residues in the [Cys^1–Cys^6] 20-membered ring. This comparison of NOESY and ROESY spectra also allows us to introduce the absence of certain cross peaks as negative constraints, as the disappearance of a cross peak cannot be due to a large variation in correlation time.

Spin diffusion constitutes a second problem for an accurate distance determination. It has been shown, however, that for transfer-NOE experiments in the fast-exchange regime the effective mixing time is equivalent to the experimentally specified mixing time multiplied by the fraction of bound ligand (Landy & Rao, 1989; Lippens *et al.*, 1992). With a typical value of 10:1 for the ratio of bound to free ligand and nominal mixing times up to 200 ms, spin diffusion is only effective over a time interval of 20 ms. For geminal protons, however, we still expect some amount of spin diffusion to occur since relaxation rates of 20 s^{-1} are expected for geminal protons in the 20-kDa complex.

We used the Tyr δ–ε proton distance as a yardstick to calibrate the other distances. A margin of ±10% was applied to give the upper and lower distance limit used as input for the distance geometry procedure. When the distance involved a proton from a geminal pair, we used a larger margin of ±20% to take into account the possibility of spin diffusion. A total of 73 NOE contacts involving protons in the six residues of the 20-membered ring were found: 39 were intraresidue contacts, 30 involved contacts between directly neighboring residues, and 4 involved protons on residues that are not direct neighbors. In comparison, one can consider the case of a globular protein such as interleukin 1β, where about 21 constraints per residue were found (Clore *et al.*, 1991). The situation is even worse for the last two residues in the tail: except for the cross peak connecting the amide protons of both residues, no interresidue cross peaks were observed.

(*b*) *Distance Geometry.* Distance geometry calculations were performed with a program made available by Dr. R. Scheek (Van Nuland *et al.*, 1992). This program allows for stereospecific assignments of the methylene protons based solely on the intensity differences of their respective cross peaks toward other protons. In order to limit the number of possible conformations, we imposed a lower distance limit of 3 Å for certain proton pairs that showed no cross peak in either the NOESY or the ROESY spectra. This improved the convergence of the algorithm, but a number of structures had the Tyr^2 side chain pointing away from the 20-membered ring, which was incompatible with the observed NOE contacts between the Tyr^2 and Asn^5 side chains. Closer investigation revealed that the problem originated from the Tyr^2 ϵ protons being subjected to no other distance restraint than the lower distance limit of 3 Å toward the Asn^5 β protons. The lack of an upper limit consistent with the chemical structure and of other triangle inequalities for the Tyr^2 ϵ protons caused the algorithm to pick a large distance between the Tyr^2 ϵ and the Asn^5 β protons. In the metric matrix method such a large distance has an important influence on the value of the resulting eigenvalues (Crippen & Havel, 1988) and thus on the overall conformation of the resulting structure. Since the large value for the Tyr^2 ϵ–Asn^5 β distance caused the tyrosine ring to turn away from the cyclic part of the molecule, with side-chain (χ_1, χ_2) angles around (–90°, –90°), strain was induced in the main chain as well, with energetically unfavorable positive ϕ angles (Richardson & Richardson, 1989) for both the Tyr^2 residue main chain and the main chains of the residues at positions 5 and 6. Moreover, the structures with the Tyr^2 ring pointing away from the cyclic moiety had *all* distances between the Tyr^2 δ and ϵ protons and the Ile^3 side chain larger than 4 Å, even though we had introduced some approximate constraints of 2–5 Å between protons on both side chains [because of an increased local mobility for the Ile^3 side chain (Nirmala *et al.*, 1992)]. A final argument for rejecting structures with an outward pointing tyrosine ring was the relation between the distances of the Tyr^2 β–Asn^5 β pair and the Tyr^2 ϵ–Asn^5 β proton pair. The constraints that we imposed $d(Tyr^2\ \beta\text{–}Asn^5\ \beta) > 3.5$ Å and $d(Tyr^2\ \delta\text{–}Asn^5\ \beta) < 4.2$ Å, are not sufficient to define a relationship between both distances, but the presence of a cross peak between the Asn^5 β and the Tyr^2 δ protons together with the absence of a cross peak for the Tyr^2 β–Asn^5 β pair implies that the Tyr^2 aromatic ring should be oriented toward the Asn^5 residue, corresponding to positive values for the χ_1 angle. We have thus retained only those structures that correspond to (χ_1, χ_2) angles around (90°, 90°) for the Tyr^2 residue.

(*c*) *Restrained Molecular Dynamics.* The distance geometry structures with the fewest NOE violations were used as starting coordinates for restrained molecular dynamics runs, performed with routines implemented in the BRUGEL package (Delhaise *et al.*, 1985). The empirical energy function describing the interatomic interactions contains terms corresponding to bond stretching, angle bending, dihedral angle, and improper dihedral angle potential terms as well as van der Waals and electrostatic terms (Wodak *et al.*, 1986). A split parabolic force law, with separate inputs for the upper and lower distance limits, was used to represent the NOE restraining force (Kaptein *et al.*, 1985). The restraint force constant was fixed at 50 kcal/(mol·Å^2) (Fesik *et al.*, 1991). Although this value seems high, one should keep in mind that the NOE restraining term here mimics the presence of the neurophysin protein. Whereas omitting this restraint force should not change the structure in a simulation of the equilibrium conformation of a solvated protein, this is not the case for the conformation of a bound ligand. A lower value of 20 kcal/mol for the restraint force constant was tested but proved to be unable to keep the oxytocin molecules reasonably close to their initial conformation, especially because the hydrogen bond term works in a sense opposite that of the NOE constraining term. As the simulations are performed *in vacuo*, where no solvent molecules are present to form hydrogen bonds with the polar groups of the peptide, the structures showed a tendency to form intramolecular hydrogen bonds. In particular, the amide proton of Asn^5 changed it position considerably in an attempt to make a *trans*-annular hydrogen bond with the carbonyl oxygen of Tyr^2.

In the performance of the simulations, velocities randomly choosen from a Maxwellian distribution for a temperature of 300 K were assigned to every atom. A 5-ps equilibration run was started, during which the velocities were rescaled every 50 molecular dynamics (MD) steps (1 step = 1 fs) to keep the temperature at its initial value. In the actual 100-ps simulations, from which the configurations were saved every 100 fs, no significant temperature drift was observed, even though no temperature control was applied.

RESULTS AND DISCUSSION

NMR Distance Restraints. A total of 101 distances were determined from the NOE experiments (see Table I). For 21 of these distances, an accurate determination as described in Materials and Methods was done. For the other peaks, problems of overlap or increased mobility (Nirmala *et al.*, 1992) made an accurate distance determination more difficult, so rather than introducing precise but incorrect distance limits, we classified them as strong (2–3 Å), medium (2–4 Å), or weak (2–5 Å). The values of the cross- and diagonal-peak volumes at different mixing times used to obtain accurate distance limits are available in the supplementary materials.

Three-Dimensional Structure of Oxytocin Bound to Neurophysin. (*a*) *Structures Obtained from the Distance Geometry Calculations.* Starting from the NOE constraints listed in Table I, we generated 32 structures with a distance geometry routine. From these we only examined seven structures with (χ_1, χ_2) angles of (90°, 90°) for the Tyr^2 residue (see Materials and Methods). No violations of the upper distance limits larger than 0.5 Å were found, and the maximal violation of the lower distance limits was 0.3 Å (see Table II). For all seven structures, the sum of all distance violations was not higher than 2 Å. Atomic coordinates of the seven structures were compared pairwise (MacLachlan, 1979) to analyze conformational differences and to obtain information about conformational flexibility (see Table II). Only a slight increase of 0.4 Å in root mean square deviation (rmsd) was observed when, rather than only the N–C^α–C′ atoms, all backbone atoms of the 20-membered ring, including the carbonyl oxygen and the backbone hydrogens, are superimposed. This increase is due to the fact that one structure has a coordinated change at the (ϕ,ψ) angles between the Gln^4 and Asn^5 residues. Including side-chain atoms of residues 1–6 in the superposition increases the rmsd by almost 1 Å. Including the last three residues of the oxytocin "tail" increases the rmsd even further, due primarily to the lack of constraints for this part of the structure. The coordinate superpositions were also carried out, considering only the part adjacent to the disulfide bridge (residues 1–2 and 5–6), because these structural elements provide the majority of contacts with the neurophysin molecule [for reviews, see Blumenstein (1984) and Breslow and Burman (1990)]. Still, no significant

Table II: Comparative Analysis of the Seven Structures with Tyr^2 (χ_1, χ_2) Angles around (90°, 90°)[a]

quantity	av ± SD (range)
Residual NOE Distance Constraints Violations	
no. of violations > 0.2 Å	3.0 ± 2.2 (0–6)
sum of violations of upper limits (Å)	1.6 ± 0.4 (1.2–2.2)
sum of violations of lower limits (Å)	0.4 ± 0.2 (0.15–0.6)
maximum upper limit violation (Å)	0.31 ± 0.10 (0.19–0.51)
maximum lower limit violation (Å)	0.19 ± 0.1 (0.05–0.34)
Av Global Pairwise rmsd	
N, C$^\alpha$, C′ of 20-membered ring	1.0 ± 0.5 (0.3–2.0)
all backbone atoms* of 20-membered ring	1.4 ± 0.5 (0.4–2.4)
all atoms of 20-membered ring	2.3 ± 0.8 (1.1–3.5)
all atoms of entire molecule	3.4 ± 0.6 (2.2–4.3)
Av Local Pairwise rmsd for [1-2-5-6]	
N, C$^\alpha$, and C′ of residues 1, 2, 5, and 6	0.9 ± 0.6 (0.2–2.0)
all backbone atoms* of residues 1, 2, 5, and 6	1.3 ± 0.6 (0.4–2.2)
all atoms of residues 1, 2, 5, and 6	1.8 ± 0.8 (0.8–3.2)

[a] Upper and lower NOE distance violations are computed as the difference between the actual distances and the corresponding distance limit (* = including the backbone hydrogens).

differences could be detected at the backbone level between the pairwise rmsd of the segments and that of the full cyclic moiety. Here, too, including the side chains increases significantly the rmsd, though less so than when the full cyclic moiety is considered. This is consistent with the earlier observation (Blumenstein, 1984; Breslow & Burman, 1990) that the side chains of residues 3 and 4 are less involved in the binding and thus could have a less well defined structure.

(*b*) *Structures Obtained after Restrained MD.* Each of the seven distance geometry structures was subjected to a restrained molecular dynamics run. Six structures started with a positive value for the angle around the disulfide bond, whereas one structure was characterized by a negative value for that angle. No change in chirality was observed during any of the MD runs. The averaged structures from the different MD runs showed even more resemblance than the starting structures. In Table III, we give the dihedral angles averaged over the six MD runs corresponding to structures with a positive chirality around the disulfide bridge. In Figure 1, we show the superposition of 10 snapshots taken along the 100-ps trajectory starting from one of these structures. Denoting the average value of a dihedral angle along one single MD trajectory by α and the standard deviation for this angle over the 100-ps run by $\Delta\alpha$, besides the global average, $\langle\alpha\rangle$, we also list in Table III the values of the deviation of α from $\langle\alpha\rangle$, $\Delta\langle\alpha\rangle$, and the average of the fluctuations along a single trajectory, $\langle\Delta\alpha\rangle$. The former indicates the differences between the averaged structures from the six MD runs; the latter, the average variation of the dihedral angle during a 100-ps MD run. Fluctuations of the structures during the 100-ps simulations were small, particularly at the level of residues 1-2-3 and 6-7, and from the values in Table III it can be seen that the variations in average dihedral angles between the different trajectories are of the same order of magnitude as the fluctuations of the dihedral angles during the individual trajectories. The backbone angles of the Gln^4 residue and the Asn^5 ϕ angle show a greater spread between the different MD runs, due to an inversion of the peptide plane for two of the six structures. Variations within every single MD run remain small, however. For the residues in the tail of the oxytocin molecule, we have large variations of dihedral angles within a single MD run, indicating a large mobility for these residues. The negative value for the angle around the disulfide bond observed in one of the structures induced important changes for this structure compared to the six others. Most important were the changes for the dihedral angles of the Tyr^2 residue [$(\phi,\psi) = (-54°, -66°)$] and the Asn5 residue [$(\phi,\psi) = (-122°, -74°)$].

The resulting energies obtained for the trajectories corresponding to the six different starting structures with a positive chirality around the disulfide bridge are given in Table IV. Typically a drop by a factor of 2–3 is observed between the total potential energy of the starting structures and the averaged energy computed over the 100-ps simulations. The main contribution to this drop in potential energy comes from the van der Waals term. This is, however, an artifact due to the difference in van der Waals radii used in the DISGEO routines and the CHARMM force field (Brooks *et al.*, 1983). In the DISGEO routines, these radii are typically 20% lower, allowing a closer approach for the atoms. The energy calculations were done with the larger van der Waals radii of the CHARMM force field, which leads to the observed large values. The average contribution of the NOE restraints term over the restrained MD runs is not dramatically different from that of the distance geometry structures. But even though this NOE contribution to the potential energy can increase during the MD run, this is always compensated for by a decrease in electrostatic and hydrogen bond energy terms.

Whereas the energy values averaged over the 100-ps trajectories are comparable for all six structures with a positive chirality around the disulfide bridge, the values of the hydrogen bond, electrostatic, and NOE distance constraint terms are less favorable by a factor of 2 for the structure with a negative chirality around the disulfide bridge. The energetic differences correlate well with the differences in average conformation and can be attributed directly to the negative torsional angle for the S–S bridge of this structure. This change of chirality of the disulfide bridge induces an increase in the NOE, hydrogen bond, and electrostatic terms at the level of the neighboring residues, resulting in a 35% increase in total potential energy for the second structure.

(*c*) *The Bound Form of Oxytocin versus the Crystal Structure.* The structure of deaminooxytocin has been determined by X-ray crystallography (Wood *et al.*, 1986). Every oxytocin molecule is hydrated by no more than seven water molecules in the wet form and by an even smaller number in the dry crystal form. Intermolecular contacts between neighboring oxytocin molecules were observed in the crystal. Examples of these crystalline contacts are the carbonyl oxygen of Cys^1, which is rotated upwards to form a hydrogen bond with the amide hydrogen of Asn^5 of a neighboring molecule, and the contact between the Tyr^2 hydroxyl and the disulfide bridge of a neighbor (Husain *et al.*, 1990).

In the crystal structure, the residues in the [Cys^1–Cys^6] ring form a short antiparallel β-pleated sheet with a β-II turn formed by residues Tyr^2 to Asn^5 (see Figure 2a). The turn contains two *trans*-annular hydrogen bonds, Tyr^2 NH–Asn^5 CO and Tyr^2 CO–Asn^5 NH. The tripeptide tail forms a β-III turn, held by a weak intramolecular hydrogen bond between Cys^6 CO and Gly^9 NH. The Tyr^2 side chain is pointing toward the Cys^1 residue and is characterized by a value for its χ_1 angle of −50°. Both chiralities for the S–S bond were found.

An earlier study on the oxytocin–neurophysin system (Hallenga *et al.*, 1988) showed in a qualitative way that oxytocin bound to neurophysin adopts a conformation distinctly different of that of deaminooxytocin in its crystalline form. Our results indicate that oxytocin bound to neurophysin loses its two *trans*-annular hydrogen bonds. The two antiparallel backbone segments 1–2 and 5–6 have their planar peptide

Table III: Dihedral Angles Defining the Backbone Conformation, the Tyr[2] and Asn[5] Side-Chain Conformations, and the Chirality of the Disulfide Bridge for the Six Structures Characterized by a Positive Chirality of the Disulfide Bridge[a]

angle	$\langle\alpha\rangle$ ($\Delta\langle\alpha\rangle/\langle\Delta\alpha\rangle$)	angle	$\langle\alpha\rangle$ ($\Delta\langle\alpha\rangle/\langle\Delta\alpha\rangle$)	angle	$\langle\alpha\rangle$ ($\Delta\langle\alpha\rangle/\langle\Delta\alpha\rangle$)	angle	$\langle\alpha\rangle$ ($\Delta\langle\alpha\rangle/\langle\Delta\alpha\rangle$)
Cys[1] ψ	165(4/9)	Gln[4] ψ	−26(83/15)	Pro[7] ψ	161(6/11)	Cys[6] χ_1	100(23/13)
Tyr[2] ϕ	−101.5(9/10)	Asn[5] ϕ	−4(86/10)	Leu[8] ϕ	−20(60/21)	Tyr[2] χ_1	99(20/15)
Tyr[2] ψ	−84.5(5/10)	Asn[5] ψ	−31(6/7)	Leu[8] ψ	54(17/23)	Tyr[2] χ_2	97(7/8)
Ile[3] ϕ	−110(5/12)	Cys[6] ϕ	−43(10/12)	Gly[9] ϕ	104(12/55)	Asn[5] χ_1	121(28/13)
Ile[3] ψ	−154(7/9)	Cys[6] ψ	121(12/19)	Gly[9] ψ	5(7/75)	S–S MD	96(7/10)
Gln[4] ϕ	−14(32/16)	Pro[7] ϕ	−71(12/14)	Cys[1] χ_1	0(53/8)	S–S DG	96(25)

[a] In parentheses are given the deviations of the individual MD structures from the global average and the average variations of the dihedral angles along the 100-ps trajectory. The last value in the table is the average angle about the S–S bridge in the DISGEO structures.

FIGURE 1: Superposition of the backbone atoms, the disulfide bridge, and the Tyr[2] side chain of 10 snapshots taken at regular intervals of 10 ps along the 100-ps restrained MD trajectory starting from the first DISGEO structure. Superposition is especially good for residues 1, 2, 5, and 6. The two residues of the tail (Leu[8] and Gly[9]) are much less restrained (data not shown). The side chain of the Tyr[2] residue shows some mobility during the simulation, but variations of the χ_1 angle remain limited to 15°, and the aromatic ring is always positioned over the 20-membered ring and keeps its orientation toward the Ile[3] residue.

Table IV: Average Conformational Energy (kcal/mol) of the Six Structures Characterized by a Positive Chirality of the Disulfide Bridge

energy	distance geometry[a]	100-ps MD run[b]
total	331(75)	174(10)
E_{vdW}	59(38)	−19(3.0)
E_{HB}	−1.9(0.6)	−5.8(0.7)
E_{elec}	18.7(2.0)	7.6(1.0)
E_{NOE}	18(11)	21.2(3)

[a] Average values and standard deviations of the starting (DISGEO) structures. [b] Values averaged over the 100-ps MD runs and standard deviations.

bonds rotated out of the plane defined by the cyclic backbone (see Figure 2b). The ring has a convex shape (Figure 1), and the turn at the Tyr[2], Ile[3], Gln[4], and Asn[5] residues cannot be characterized as a type I, II, or III β-turn. The Tyr[2] side chain has changed its orientation. Whereas in the crystal structure it points toward the Cys[1] residue, in the bound form it points toward the Ile[3] residue ($\chi_1 = 90°$).

As was already observed in a former transfer-NOE study of the oxytocin–neurophysin complex (Nirmala, 1987), numerous NOE distance constraints measured for oxytocin bound to neurophysin are violated in the crystal structure of oxytocin. In Table V, we give the most important differences between distances of proton pairs in the crystal structure and in our model for the bound oxytocin. The distances in our model were calculated as $\langle r^{-3}\rangle^{-1/3}$ rather than as $\langle r^{-6}\rangle^{-1/6}$ averages over the 100-ps trajectory of the first structure, because the NOE effect is determined by dipolar interactions that persist over the time scale of the rotational motion of the molecule (Tropp, 1980; Kessler *et al.*, 1988). Fast fluctuations on the picosecond time scale of the MD simulation do not contribute significantly and will be averaged out.

Binding to Neurophysin. (a) The Peptide α-Amino Group. The importance of the peptide α-amino group of oxytocin for binding to neurophysin was first recognized by the failure of deaminooxytocin to bind to neurophysin (Stouffer *et al.*, 1963). It was also shown that its p*K* is elevated by at least 5 pH units in the complex relative to the unliganded state, consistent with the formation of a salt bridge in a nonpolar environment (Blumenstein *et al.*, 1977). In our bound conformation, the α-amino group is sticking outwards and forms no interactions with the rest of the peptide. This arrangement would allow it to readily form such a salt bridge with neurophysin. It is, however, unlikely that this bridge is present under our experimental conditions, which require a pH of 2.1 to prevent aggregation, precluding the presence of a charged carboxylic acid on the protein surface.

(b) Backbone Atoms of the Cycle. The situation of slow exchange on the chemical shift time scale is found for protons in the cyclic part of the molecule, and only in residues 1–2 and 5–6 (see Table VI). This is in agreement with the earlier findings that the "tail" of the molecule is relatively less important for binding and therefore will experience only minor chemical shift changes. It also confirms earlier work (Live *et al.*, 1987), in which isotope enrichment was used to evaluate the chemical shifts of the amide ^{15}N resonances in the free and bound form.

The backbone conformations of the Cys[1]–Tyr[2]–Ile[3] and Cys[6]–Pro[7] segments converge resonably well for all six conformers (Figure 1). The good convergence of the different structures at this level confirms the hypothesis that the intermolecular contacts constrain this part to a well-defined conformation with less mobility.

Thermodynamic studies of the binding of systematically modified dipeptide amides to the hormone binding site on neurophysin have provided specific evidence (Whittakker *et al.*, 1985) that the peptide bond between residues 2 and 3 of those small ligand peptides is hydrogen-bonded to the protein. In our structures, the carbonyl oxygen of Tyr[2] is indeed directed

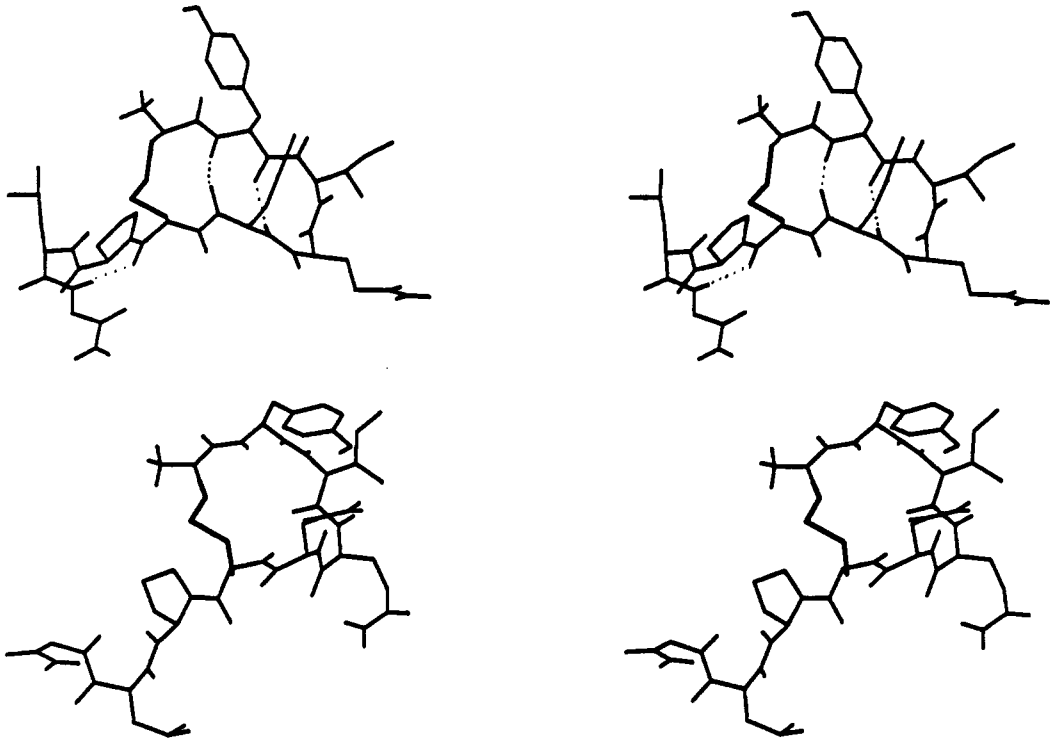

FIGURE 2: Stereoviews of (a, top) the crystal structure of deaminooxytocin and (b, bottom) the NMR-derived conformation of the bound oxytocin molecule. The latter structure is one of the snapshots along the 100-ps trajectory starting from the first structure. Whereas the crystal structure is characterized by two *trans*-annular hydrogen bonds (dotted lines) between the Tyr^2 and Asn^5 residues and by a (weak) hydrogen bond between the Cys^6 CO and the Gly9 NH, the two antiparallel backbone segments 1–2 and 5–6 in the bound conformation have their planar peptide bonds almost perpendicular to the cyclic moiety. This moiety itself is more convex in the bound form than in the crystal conformation.

Table V: Average Distances between Proton Pairs in the Crystal Structure and along the MD Trajectory of Structure 1[a]

	distance (Å)			distance (Å)	
proton pair	crystal	MD	proton pair	crystal	MD
Cys^1 α–Cys6 α	2.9	4.2	Tyr^2 H–Ile^3 H	4.4	2.8
Tyr^2 H–Cys6 α	3.3	5.1	Tyr^2 H–Asn^5 β_1	5.3	3.6
Cys^1 β_1–Tyr^2 H	4.5	3.4	Tyr^2 H–Asn^5 β_2	6.0	4.1
Cys^1 β_2–Tyr^2 H	3.8	2.5	Tyr^2 δ–Asn^5 β	4.6	3.9
Cys^1 β_1–Cys^6 α	5.4	3.0	Ile^3 β–Gln^4 H	4.4	2.7
Cys^1 β_2–Cys^6 α	5.6	3.8			

[a] The first two distances are shorter in the crystal and should give rise to cross peaks in the NMR spectrum. The other distances are larger than 3.5 Å in the crystal, although cross peaks are observed in the bound oxytocin conformation.

Table VI: Resonance Frequencies of Free and Bound Protons in Slow Exchange on the Chemical Shift Difference Scale

proton	ω_{IF}	ω_{IB}	proton	ω_{IF}	ω_{IB}
Cys^1 α	4.26	4.15	Asn^5 NH	8.34	8.71
Tyr^2 NH	8.99	8.80	Asn^5 β_1,β_2	2.86	3.01
Tyr^2 ϵ	6.86	6.31	Cys^6 NH	8.22	7.86
Ile^3 γ_1	1.26	1.61			

to the outer part of the cycle, allowing the formation of a hydrogen bond with a donor group on the protein. However, the constraints imposed by the NOE cross peaks between the amide proton of Ile^3 and the β and δ protons of Tyr^2 direct this amide proton inwards of the 20-membered ring, which makes a hydrogen bond with the protein more difficult.

The backbone angles of the Gln^4 residue and the Asn^5 ϕ angle show a greater spread between the different structures, and it is at those residues that we also find the largest NOE distance violations. For the first five structures, the distance between the Gln^4 and Asn^5 NH protons is around 3 Å, despite the lower limit of 3.5 Å we imposed on grounds of the absence of a cross peak between the protons. Of course, a lower relaxation rate due to either local mobility or contacts between the Asn^5 NH proton and relaxation centers on the protein (Nirmala *et al.*, 1992) might be responsible for the fact that we do not see a cross peak. The sixth and seventh structures do not show a violation of this negative restraint, but the (ϕ, ψ) angles of the Asn^5 residue are in energetically less favorable regions (positive ϕ angles) of the Ramachandran plot for both structures.

(*c*) *Importance of the Side Chains.* For the free oxytocin in aqueous solution, the rotamer populations (characterized by the angle χ_1) of different side-chain groups have been determined previously (Meraldi et al., 1977). However, the side-chain conformations in the free hormone are generally rapidly interconverting and as such would give little information about the conformations that occur in the complex. Experimental evidence for this came from the shifts in the α carbon frequencies of residues 1, 2, 4, and 6 upon binding of oxytocin enriched in ^{13}C at these positions. These shifts were attributed to changes in side-chain conformations (Blumenstein et al., 1984), although a strain in the sp^3 geometry of the C$^\alpha$ proton of the hormone residues was also invoked.

The Tyr^2 side chain of free oxytocin in aqueous solution is characterized by populations of 50% for $\chi_1 = -60°$, 32% for $\chi_1 = \pm 180°$ and 18% for $\chi_1 = 60°$ (Meraldi *et al.*, 1977). We have given arguments above in favor of a χ_1 value of 90°, indicating a large conformational change for this side chain upon binding. The value of 90° does not correspond to an energetic minimum for the side-chain conformation, but this increased energy can be compensated by a favorable interaction with the protein. Considering the importance of the Tyr^2 side chain for binding and the strongly decreased rotation rate of the aromatic ring upon interaction with NP (Blumenstein *et al.*, 1980), this deviation from the minimal energy conformation is not surprising. Competitive binding studies (Breslow

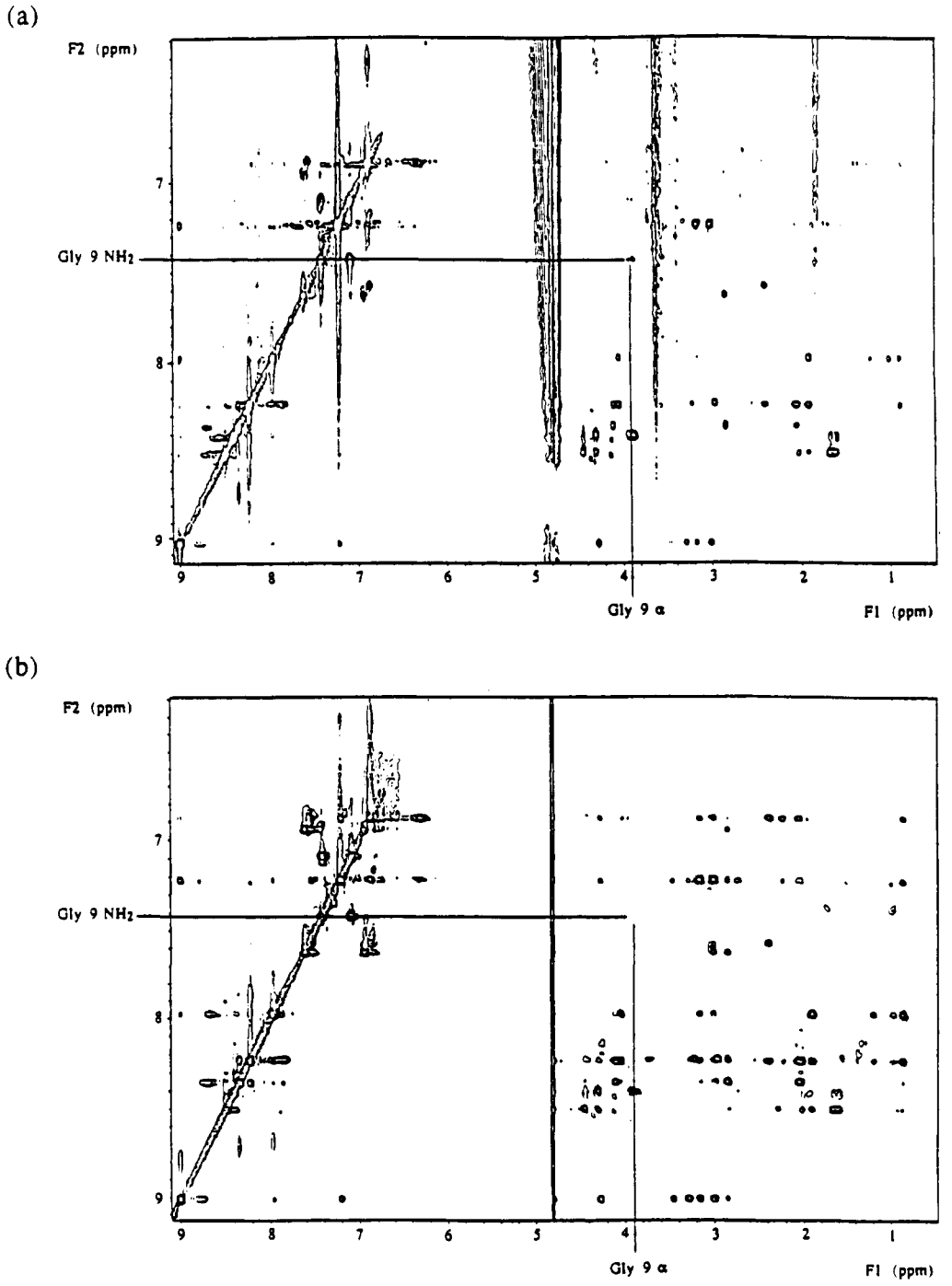

FIGURE 3: (a) NOESY spectrum with 240-ms mixing time, and (b) ROESY spectrum with 120-ms mixing time, of a sample with a 10:1 oxytocin/neurophysin ratio. The cross peak between Gly^9 α and Gly^9 NH_2 is only present in the ROESY spectrum due to residual flexibility of this residue in the oxytocin–neurophysin complex.

& Abrash, 1966) showed indeed that substitution of the Tyr residue at position 2 by Gly, Ile, or D-Tyr reduced binding to neurophysin to undetectable levels. In contrast, binding was essentially unaffected by substitution of Tyr by Phe. In the next paragraph, describing intermolecular cross peaks between residues on the oxytocin and residues on the neurophysin, we will show direct evidence of close contact of this Tyr^2 aromatic side chain with an aromatic side chain of the protein.

The side chain in position 3 was shown previously also to be implicated in the binding. Upon interaction of oxytocin with its carrier the Ile^3 side chain gets buried in a rather loose hydrophobic pocket (Breslow & Burman, 1990). This pocket does not seem to discriminate between an Ile in position 3 (as in oxytocin) and a Phe (as in vasopressin), and it also binds the corresponding D-amino acids in this position, albeit with lower affinity. A comparison of the spectra at 600 and 400 MHz revealed direct evidence for a large residual mobility of this side chain: in the NOESY spectrum at 600 MHz, a clear cross peak between the Ile^3 β proton and the Gln^4 NH proton was seen, whereas it was present with only 20% intensity in the NOESY spectrum at 400 MHz with the same mixing time (200 ms) (Mirmala *et al.*, 1992). Still, the orientation of the side chain was determined by finding out which methyl group (the δ or the γ CH_3) points toward the Gln^4 residue and which one points toward the Ile^3 amide proton. The two methyl groups can easily be distinguished in a high-resolution 1D spectrum, as the γ CH_3 group is a doublet and the δ CH_3 is a triplet. In a 2D spectrum, however, the intense methyl signals

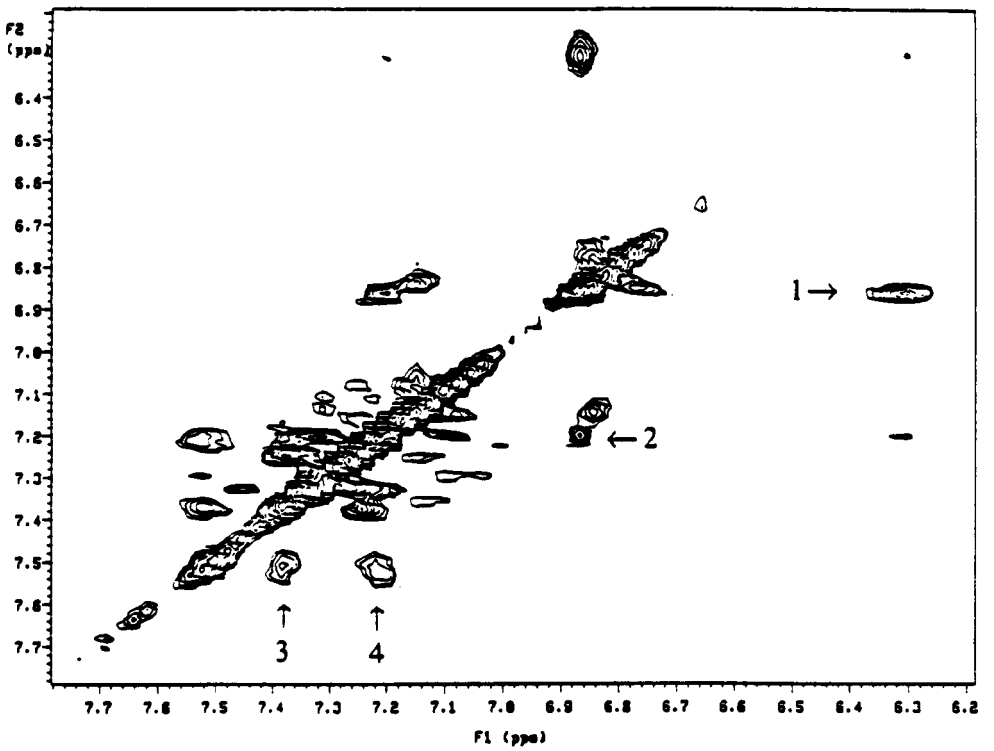

FIGURE 4: NOESY spectrum of a sample with a 3:1 oxytocin/neurophysin ratio in 99% D_2O. The cross peaks are the exchange cross peak between Tyr^2 ϵ_b and ϵ_f (1), NOE cross peaks between the δ and ϵ protons of the oxytocin Tyr^2 aromatic ring (2) and the neurophysin Phe^{22} aromatic ring (3), and an intermolecular cross peak between oxytocin Tyr^2 δ and neurophysin Phe^{22} (4).

always gave a sizeable t_1 noise streak, and the resolution in the ω_1 direction was not sufficient to determine the fine structure of the cross peak. The presence of a cross peak between the γ CH_2 protons of Ile^3 and its own amide proton indicated that the δ CH_3 group is directed toward the Ile amide proton rather than the Gln^4 residue. This was confirmed by a ROESY spectrum at 5 °C, where the difference in resonance frequency between the methyl groups was slightly larger.

The Asn^5 side chain is rather well constrained in our structures, with $-90° < \chi_1 < -180°$. The side chain is constrained into this conformation by the *trans*-annular contacts of its β protons toward the Tyr^2 residue. A comparison with the Asn^5 χ_1 populations of free oxytocin in aqueous solution of 12%, 44%, and 44% for $\chi_1 = -60°, \pm 180°$, and 60° (Meraldi *et al.*, 1977) indicates that an important change has occurred in the side-chain conformation upon binding.

Evidence for an important role in binding of the side chain in position 1 of the hormone comes from binding studies of small peptides (Breslow *et al.*, 1971), which indicate a systematic relationship between the identity of this side chain and binding affinity. Peptides with Phe in position 1 were found to be particularly good ligands, which was rationalized as being due to the aromatic ring taking the place of the disulfide bridge of the natural hormone. In crystalline oxytocin, both chiralities of the disulfide bridge are observed. Our structural data, however, indicate preferentially a 100° righthanded conformation for the bound structure. Circular dichroism studies (Urry & Walter, 1971) of free oxytocin in aqueous solution also suggested a right-handed screw sense for the disulfide bridge, and this conformation may well be stabilized by the interactions with the protein. However, for agonist versus antagonist biological activity at the uterine oxytocin receptor, different chiralities of the disulfide bond appear to be important [see Hruby (1987) for a discussion].

(*d*) *Importance of the Tail upon Binding.* While similarity of the six structures is very good for the cyclic moiety and the Pro^7 residue, the other two residues of the tripeptide tail show much larger variations. The importance of the proline residue at position 7, which we find invariably in the *trans* conformation, has to our knowledge not yet been investigated. However, a recent study detected 10% of the oxytocin molecules in aqueous solution in a *cis* conformation across the Cys^6–Pro^7 bond (Larive *et al.*, 1992). The resonances of the *cis* isomer were found to be obscured by the much more intense resonances of the *trans* isomer. In the presence of neurophysin, the strong NOE contact between the Cys^6 α and the Pro^7 δ protons is characteristic for the *trans* form, but due to the important background signals of the protein, the possibility does remain that we did not find the signals associated with the *cis* form, which in any case would only be present as a small population.

The importance of the tripeptide tail was evaluated by using oxytocin uniformly enriched in ^{13}C at the Leu^8 position by Griffin *et al.* (1977) and at the Gly^9 position by Blumenstein and Hruby (1976). They concluded that the chemical shifts of the carbons were not affected by binding to neurophysin. We provide an alternative method for the measurement of residual mobility in a bound peptide, based on the frequency dependence of the cross relaxation rate. In the ROESY spectrum (Figure 3a), a clear cross peak between the Gly^9 α and the Gly^9 NH_2 appears, but this cross peak is missing in the corresponding NOESY spectrum (Figure 3b), even though we used twice as long a mixing time for the latter. This can be understood from the relation between the cross relaxation rate and the effective correlation time, τ_c, for the dipolar interaction autocorrelation functions (Abragam, 1986). In this particular case, the C-terminal NH_2 group keeps its full mobility, giving a value of τ_c around 0.3 ns. The cross-relaxation rate in the NOESY spectrum reduces to zero, whereas it remains nonzero in the ROESY spectrum. Therefore, without the use of isotope labels, we can confirm the flexibility of this last residue.

(*e*) *Contacts between the Protein and the Peptide.* All experimental data presented so far pertain to the conformation of the oxytocin molecule bound to neurophysin. Information about the neurophysin residues involved in this binding is harder to obtain because of the overlap and the large line width of the proton resonances of the neurophysin (NP) dimer. Both factors also explain why essentially no assignments of neurophysin resonances have been made. An exception are the aromatic residues of the NP molecule, because they are limited in number (one tyrosine at position 49 and two phenylalanines at positions 22 and 35) and because their resonances fall in an otherwise empty region of the spectrum. Perdeuterated peptides containing at least one aromatic residue were used by Peyton *et al.* (1987) to study the ring-current shifts of the protein Tyr^{49} resonances caused by the binding of the aromatic cycle of the peptides. Their observations provided a partial model of the NP–oxytocin complex that places the ring of Tyr^{49} at a distance of 5–10 Å from residue 1 of the bound peptide. Clear evidence that the Tyr^2 residue of oxytocin is in the neighborhood of an aromatic side chain on the protein is given by the chemical shift difference of the Tyr^2 ϵ protons upon binding (see Table VI). Whereas the change in orientation of the *peptide* aromatic ring might be responsible for frequency differences between the bound and the free form of residues other than Tyr^2, this cannot be the case for protons on the aromatic side chain itself. Since this chemical shift difference is not necessarily related to the presence of another aromatic ring, however, another experiment was performed with a peptide/protein ratio of 3:1 in D_2O. This lower excess concentration of peptide over protein allows a better observation of resonances of protein protons in the complex. The aromatic region of this spectrum is shown in Figure 4. Four types of cross peaks are visible in this spectrum: (a) the *intra*aromatic cross peaks (between meta and ortho protons) of one of the three aromatic residues on the protein, (b) the same *intra*aromatic cross peaks for the Tyr^2 side chain of oxytocin, (c) the exchange peak between the ϵ protons of the Tyr^2 residue in the bound and free forms, and (d) a last peak which is an *inter*molecular NOE between a Tyr^2 δ proton of the oxytocin and an aromatic proton of the protein. The resonances of the Tyr^{49} residue of NP have been assigned to 6.79 ppm for the ϵ protons and 7.10 ppm for the δ protons (Peyton *et al.*, 1987). These resonances change little when a Phe-Phe-NH_2 or Phe-Phe-Leu-NH_2 peptide is added; as the binding of these peptides is very similar to that of oxytocin (Breslow & Burman, 1990), it is most probable that neither will the binding of oxytocin cause major shifts. This leaves only the three Phe residues of NP as candidates for the proton signals indicated by cross peak 3 in Figure 4. The recently obtained crystal structure of a neurophysin II–I-Phe-Tyr-NH_2 complex shows that Phe^{35} is at the interface between the two NP monomers, far away from the dipeptide binding site. Phe^{91} is in the C-terminal part of neurophysin, a highly disordered region in the crystal structure. Although an interaction between Phe^{91} and oxytocin cannot be excluded entirely, we tentatively conclude that the Tyr^2 ring of oxytocin is very close in space to the aromatic ring of neurophysin Phe^{22}. This provides us with an anchoring point for the oxytocin molecule when it binds to neurophysin and should allow us to derive a detailed atomic model of the complex by molecular modeling techniques.

CONCLUSIONS

We conclude from our model for the oxytocin molecule bound to neurophysin that it undergoes important conformational changes upon interaction. The crystal structure of the free molecule is not an accurate description of the conformation in the complex. A next step will be to study its conformation when it interacts with a receptor protein rather than with its carrier neurophysin.

The present study has shown the potential of transfer-NOE techniques to derive an accurate structure of a ligand in its bound state and can probably be extended to many other systems where the ligand interacts weakly with its target molecule.

SUPPLEMENTARY MATERIAL AVAILABLE

Tables listing values of the cross- and diagonal-peak volumes at different mixing times used to obtain accurate distance limits (6 pages). Ording information is given on any current masthead page.

REFERENCES

Abragam, A. (1986) *Principles of Nuclear Magnetism*, Clarendon Press, Oxford.

Amit, A. G., Mariuzza, R. A., Phillips, S. E. V., & Poljak, R. J. (1986) *Science 233*, 747.

Anglister, J., & Zilber, B. (1990) *Biochem. 29*, 921.

Artymiuk, P. D., Blake, C. C., Grace, D. E., Oatly, S. J., Philips, D. C., & Sternberg, M. J. (1979) *Nature 280*, 563.

Balaram, P., Bothner-By, A. A., & Dadok, J. (1972a) *J. Am. Chem. Soc. 94*, 4015.

Balaram, P., Bothner-By, A. A., & Dadok, J. (1972b) *J. Am. Chem. Soc. 94*, 4017.

Bennett, W. S., & Huber, R. (1984) *Crit. Rev. Biochem. 15*, 291.

Bevilacqua, V. L., Thomson, D. S., & Prestegard, J. H. (1990) *Biochemistry 29*, 5529.

Blow, D. M. (1976) *Acc. Chem. Res. 9*, 145.

Blumenstein, M. (1984) in *Conformation in Biology and Drug Design*, Vol. 7, *The Peptides. Analysis, Synthesis, Biology* of (Hruby, V. J., Ed.) Academic Press, New York.

Blumenstein, M., & Hruby, V. J. (1976) *Biochem. Biophys. Res. Commun. 68*, 1052.

Blumenstein, M., Hruby, V. J., Yamamoto, D., & Yang, Y. (1977) *FEBS Lett. 81*, 347.

Blumenstein, M., Hruby, V. J., Viswanatha, V. (1979) *Biochemistry 18*, 3553.

Blumenstein, M., Hruby, V. J., & Viswanatha, V. (1980) *Biochem. Biophys. Res. Commun. 94*, 431.

Blumenstein, M., Hruby, V. J., Viswanatha, V., & Chaturvedi, D. (1984) *Biochemistry 23*, 2153.

Bothner-By, A. A., Stephens, R. L., Lee, J., Warren, C. D., & Jeanloz, R. W. (1984) *J. Am. Chem. Soc. 106*, 811.

Breslow, E. (1979) *Annu. Rev. Biochem. 48*, 251.

Breslow, E., & Abrash, L. (1966) *Proc. Natl. Acad. Sci. U.S.A. 56*, 640.

Breslow, E., & Burman, S. (1990) *Adv. Enzymol. Relat. Areas Mol. Biol. 63*, 1.

Breslow, E., Aanning, H. L., Abrash, L., & Schmir, M. (1971) *J. Biol. Chem. 246*, 5170.

Breslow, E., Weis, J., & Menendez-Botet, C. J. (1973) *Biochemistry 12*, 4644.

Brewster, A. I., & Hruby, V. J. (1973) *Proc. Natl. Acad. Sci. U.S.A. 70*, 3806.

Brewster, A. I., Hruby, V. J., Spatola, A. F., & Bovey, F. A. (1973) *Biochemistry 12*, 1643.

Brooks, C. L., III, Bruccoleri, R. E., Olafson, B. D., States, D. J., Swaminathan, S., & Karplus, M. (1983) *J. Comput. Chem. 4*, 187.

Campbell, A. P., & Sykes, B. D. (1991) *J. Mol. Biol. 222*, 405.

Capra, J. D., Kehoe, J. M., Kotelchuck, D., Walter, R., & Breslow, E. (1972) *Proc. Natl. Acad. Sci. U.S.A. 69*, 431.

Chen, L., Rose, J. P., Breslow, E., Yang, D., Chang, W.-R., Furrey, W. F., Sax, M., & Wang, B.-C. (1991) *Proc. Natl. Acad. Sci. U.S.A. 88*, 4240.

Clore, G. M., & Gronenborn, A. M. (1982) *J. Magn. Reson. 48*, 402.
Clore, G. M., & Gronenborn, A. M. (1983) *J. Magn. Reson. 53*, 423.
Clore, G. M., Wingfield, P. T., & Gronenborn, A. M. (1991) *Biochemistry 30*, 2315.
Crippen, G. M., & Havel, T. F. (1988) *Distance Geometry and Molecular Conformation*, Research Studies Press Ltd., U.K.
Delhaise, P., Van Belle, D., Bardiaux, M., Hamers, P., Van Cutsem, E., & Wodak, S. J. (1985) *J. Mol. Graphics 3*, 116.
Fejzo, J., Zolnai, Z., Macura, S., & Markley, J. (1990) *J. Magn. Reson. 88*, 93.
Fesik, S. W., Gampe, R. T., Eaton, H. L., Gemmecker, G., Olejniczak, E. T., Neri, P., Holzman, T. F., Eagan, D. A., Edalji, R., Helgrich, R., Hochlowski, J., & Jackson, M. (1991) *Biochemistry 30*, 6567.
Fremont, D. H., Matsumura, M., Stura, E. A., Peterson, P. A., & Wilson, I. A. (1992) *Science 257*, 919.
Gainer, H., Russell, J. T., & Loh, Y. P. (1985) *Neuroendrocinology 40*, 171.
Griffin, J. H., DiBello, C., Alazard, R., Nicolas, P., & Cohen, P. (1977) *Biochemistry 16*, 4194.
Hallenga, K., & Koenig, S. (1976) *Biochemistry 15*, 4255.
Hallenga, K., Nirmala, N. R., Hruy, V. H., & Smith, D. D. (1988) in Proceedings, 10th American Peptide Symposium, May 1987 (Marshall, G. R., Ed.) p 39, ESCOM, Leiden.
Hendrickson, W. A., & Wüthrich, K. (1992) *Macromolecular Structures 1192*, Current Biology Ltd., London, U.K.
Hruby, V. J. (1974) in Chemistry and Biochemistry of Amino Acids, Peptides and Proteins (Weinstein, B., Ed.) pp 1–88, Marcel Decker, Vol. 3, New York.
Hruby, V. J. (1987) *Trends Pharmacol. Sci. 8*, 336.
Hubbard, S. J., Campbell, S. F., & Thomton, J. M. (1991) *J. Mol. Biol. 220*, 507.
Huber, R., & Bode, W. (1978) *Acc. Chem. Res. 11*, 114.
Husain, J., Blundell, T. J., Cooper, S., Pitts, J. E., Tickle, I. J., Wood, S. P., Hruby, V. J., Buku, A., Fischman, A. J., Wyssbrod, H. R., & Mascarenhas, Y. (1990) *Philos. Trans. R. Soc. London B 327*, 625.
Ikura, M., Clore, M. G., Gronenborn, A. M., Zhu, G., Klee, C. B., & Bax, A. (1992) *Science 256*, 632.
Jorgensen, W. L. (1991) *Science 254*, 954.
Kaptein, R., Zuiderweg, E. R. P., Scheek, R. M., Boclens, R., & Van Gunsteren, W. F. (1985) *J. Mol. Biol. 191*, 523.
Kazmierski, W. M., Yamamura, H. I., & Hruby, V. J. (1991) *J. Am. Chem. Soc. 113*, 2275.
Kessler H., Griesinger, C., Lautz, J., Müller, A., van Gunsteren, W. F., & Berendsen, H. J. C. (1988) *J. Am. Chem. Soc. 110*, 3393.
Knappenberg, M., Michel, A., Scarso, A., Brison, J., Zanen, J., Hallenga, K., Deschrijver, P., & Van Binsl, G. (1982) *Biochim. Biophys. Acta 700*, 229.
Knighton, D. R., Zheng, J., Ten Eyck, L. F., Xuong, N., Taylor, S. S., & Sodawski, J. M. (1991) *Science 253*, 414.
Landy, F. G., & Rao, B. D. (1989) *J. Magn. Reson. 81*, 379.
Larive, C. K., Guerra, L., & Rabenstein, D. L. (1992) *J. Am. Chem. Soc. 114*, 7331.
Lippens, G., & Hallenga, K. (1990) *J. Magn. Reson. 88*, 619.
Lippens, G., Cerf, C., & Hallenga, K. (1992) *J. Magn. Reson. 99*, 268.
Live, D. H., Cowburn, D., & Breslow, E. (1987) *Biochemistry 26*, 6415.
MacLachlan, A. D. (1979) *J. Mol. Biol. 128*, 49.
Macura, S., Farmer, B. T., II, & Brown, L. R. (1986) *J. Magn. Reson. 70*, 493.
Meraldi, J.-P., Hruby, V. J., & Brewster, A. I. (1977) *Proc. Natl. Acad. Sci. U.S.A. 74*, 1373.
Ni, F., Konishi, Y., Bullock, C. D., Rivetna, M. N., & Scheraga, H. A. (1989) *Biochemistry 28*, 3106.
Ni, F., Konishi, Y., & Scheraga, H. A. (1990) *Biochemistry 29*, 4479.
Nirmala, N. R. (1987) Ph.D. Thesis, Michigan State University.
Nirmala, N. R., Lippens, G., & Hallenga, K. (1992) *J. Magn. Reson. 100*, 25.
Peyton, D., Sardana, V., & Breslow, E. (1987) *Biochemistry 26*, 1518. Pople, J. A., Schneider, W. G., & Bernstein, H. J. (1959) *High-resolution Nuclear Magnetic Resonance*, p 221, McGraw-Hill, New York.
Puglisi, J. D., Tan, R., Calnan, B. J., Frankel, A. D., & Williamson, J. R. (1992) *Science 257*, 76.
Richardson, J. S., & Richardson, D. C. (1989) in *Prediction of Protein Structure and the Principles of Protein Conformation* (Fasman, G., Ed.) pp 43–72, Plenum Press, New York.
Rini, J. M., Schulze-Gahmen, U., & Wilson, I. A. (1992) *Science 255*, 959.
Stouffer, J. E., Hope, D. B., & du Vigneaud, V. (1963) in *Perspectives in Biology* (Cori, C. F., Foglia, G., Lcloir, L. F., Ochoa, S., Eds.) p 75, Elsevier, Amsterdam.
Tropp, J. (1980) *J. Chem. Phys. 72*, 6035.
Upson, D. A., & Hruby, V. J. (1976) *J. Org. Chem. 41*, 1353.
Urry, D. W., & Walter, R. (1971) *Proc. Natl. Acad. Sci. U.S.A. 68*, 956.
van Nuland, N. A., Grötzinger, J., Dijkstra, K., Scheek, R., & Robillard, G. T. (1992) *Biochemistry* (submitted for publication).
Wagner, G., Braun, W., Havel, T. F., Schaumann, T., Go, N., & Wüthrich, K. (1987) *J. Mol. Biol. 196*, 611.
Weber, C., Wider, G., von Freyberg, B., Traber, R., Braun, W., Widmer, H., & Wüthrich, K. (1991) *Biochemistry 30*, 6563.
Weber, P. C., Ohlendorf, D. H., Wendolowski, J. J., & Salemme, F. R. (1991) *Science 243*, 85.
Whittaker, B. A., Allewell, N. M., Carlson, J., & Breslow, E. (1985) *Biochemistry 24*, 2782.
Wodak, S. J., Decoen, J.-L., Edelstein, S. J., Demarne, H., & Beuzard, Y. (1986) *J. Biol. Chem. 261*, 14717.
Wood, S. P., Tickle, I. J., Treharne, A. M., Pitts, J. E., Mascarenhas, Y., Ly, J. I., Husain, J., Cooper, S., Blundell, T. L., Hruby, V. J., Buku, A., Fischman, A. J., & Wyssbrod, H. R. (1986) *Science 232*, 633.